Theoretical atomic-force-microscopy study of adsorbed fullerene molecules

C. Girard and X. Bouju
Laboratoire de Physique Moléculaire, F-25030 Université de Franche Comté, Besançon Cedex, France

O. J. F. Martin
IBM Research Division, Zurich Research Laboratory, Säumerstrasse 4, CH-8803 Rüschlikon, Switzerland

A. Dereux
Institute for Studies in Interface Sciences, Facultés Universitaire Notre-Dame de la Paix, 61 rue de Bruxelles, B-5000 Namur, Belgium

C. Chavy, H. Tang, and C. Joachim
Centre d'Elaboration des Materiaux et d'Etudes Structurales,
29 rue Jeanne Marvig, Boîte Postale 4347, F-31055 Toulouse Cedex, France
(Received 15 June 1993)

The capability of atomic-force microscopy (AFM) to localize both individual adsorbates and aggregates of adsorbed molecules was demonstrated a few years ago. More recently submonolayers of fullerene molecules deposited on a gold substrate have been imaged using such devices. In this paper, simulations of the atomic force between a thin probe tip and a set of adsorbed molecules is presented. The long-range part of the interaction is determined from a whole self-consistent procedure in which many-body effects are accounted for at all orders. In this description the probe tip interacts with the molecules and the surface through many-body dispersion forces. Short-range interactions are then included by using an atom-atom semiempirical pairwise potential. Simulations of AFM images of C_{60} adsorbed molecules are presented in two different modes of imaging: the constant-tip-height mode and the constant-force mode.

I. INTRODUCTION

The advent of local probe microscopies makes available a growing number of measurements of structures stabilized on clean and covered surfaces.[1,2] Very recently, important new issues have arisen with the development of atomic force microscopy (AFM).[3] This technique derives from scanning tunneling microscopy (STM) and consists of measuring the force or the deflection between a thin probe tip and the sample surface. The probe-surface distance can be varied within a few angstroms up to about 100 nm. Therefore, in AFM, two different regimes can be defined.[4,5] In the first one, strong repulsive forces monitored with a very sharp probe tip allow atomic resolution to be reached. By increasing the working distance, the attractive regime corresponding to long-range interactions (van der Waals, electrostatic, etc.) can be used for imaging larger structures (tracks, steps, surface defects, or biological molecules).

Since the original paper of Binnig, Quate, and Gerber,[3] many surface corrugations with subnanometer resolution have been recorded. In addition to observing structures at the atomic level, the AFM has successfully imaged surfaces with adsorbed molecules, such as sorbic acid, Langmuir-Blodgett films, and proteins.[6] More recently, results of AFM studies on a submonolayer coverage of C_{60} on gold surface have been reported by Sarid *et al.* and by Dietz *et al.*[7,8] As described in these papers, AFM can directly measure the tip-sample forces and in this case the corresponding images reflect the spatial distribution of the total charges of the fullerene molecules that are responsible for the forces involved in the AFM imaging process.

The operation modes of the AFM devices are influenced by a number of different physical aspects related to the interaction between two solid bodies.[4,5] Therefore understanding the physical processes at the origin of the image formation requires specific models adapted to the low symmetry of the tip-sample system.[9–12] As said above, the sign and the character of the force varies according to the value of the tip-surface separation. The most prominent repulsive force is due to the overlap of electron clouds. This force may be directional or anisotropic and in any case varies strongly as a function of the distance. At large distances, the van der Waals forces are the sole sources of interaction between two neutral electrodes.[11,12] Since the pioneering works of Lifshitz it is well known that the existence of such long-range effects originates in the correlations between the fluctuations of the charges densities inside the two interacting media.[13]

The aim of the present paper is twofold. First, a unified treatment of the long-range interaction between a set of adsorbed molecules and an AFM probe tip is described. The long-range part of the interaction is determined from a fully self-consistent procedure in which many-body effects are introduced at all orders.[14] More precisely, we will start by building the response of a coated surface from a sequence of Dyson's equations. In a second stage, in order to simulate AFM images of fullerene molecules, the short-range part will then be introduced by considering a summation of pairwise atomic po-

tentials. Numerical results on C_{60} molecules will be presented in two different modes of imaging: the constant tip-height mode and the constant-force mode. Comparisons with recent experimental results will be proposed.

II. THE TIP-SAMPLE SYSTEM

We consider in this section the problem of an AFM probe-tip placed above a set of (p) molecules deposited upon a plane surface. The geometry of the model is shown in Fig. 1. The structure of the tip apex described atom by atom is composed of four layers of atoms with a C_{3v} symmetry. This tip structure was already used to reproduce with good agreement experimental AFM images of graphite by using a fully relaxed molecular mechanical approach.[15] When such a probe tip is placed close to the coated surface, the long-range interaction energy U_d due to the electric correlations between the charges density fluctuations gives rise to an attractive force. At very short distances, this force becomes repulsive because of the overlapping of the electronic clouds of the tip and sample. In order to account for this contribution, we will assume between each atom composing the tip apex and each atom of the adsorbed molecules a pairwise potential of the form

$$U_r(\mathbf{r}_i,\mathbf{R}_j)=C_{12}/|\mathbf{r}_i-\mathbf{R}_j|^{12} , \tag{1}$$

where the short-range parameters C_{12} characterizing this form are generally available in the literature for many atom pairs.[16]

A. The dispersion energy

One of the difficulties in formulating a theory for the van der Waals dispersion interactions between two extended systems lies in the fact that van der Waals effects have a many-body character. Thus, in the past, two general approaches have been adopted to account for this feature. In one class, the interaction is formulated in terms of the properties of the individual systems by considering their correlated charge fluctuations.[17] In the second class, the material bodies are treated in terms of their collective properties.[18] In other words, the latter method is based on the existence of the coupled electromagnetic modes occurring when the two systems interact. As discussed in Ref. 19, the coupled modes method provides a convenient framework for describing the dispersion energy U_d between an AFM probe tip and a coated surface: the coupled modes between an n-atom tip apex and the sample are the solutions of a standard dispersion relation

$$D(\omega)=\det[\underline{I}-\underline{B}(\mathbf{R}_0,\omega)]=0 , \tag{2}$$

where $\underline{I}$ represents the identity matrix, $\mathbf{R}_0$ the position vector of the atom terminating the tip apex, and $\underline{B}$ is the $(3n\times 3n)$ matrix defined by

$$\underline{B}(\mathbf{R}_0,\omega)=\alpha(\omega)\begin{bmatrix} \mathbf{S}(\mathbf{R}_1,\mathbf{R}_1,\omega) & \mathbf{S}(\mathbf{R}_1,\mathbf{R}_2,\omega) & \cdots & \mathbf{S}(\mathbf{R}_1,\mathbf{R}_n,\omega) \\ \mathbf{S}(\mathbf{R}_2,\mathbf{R}_1,\omega) & \mathbf{S}(\mathbf{R}_2,\mathbf{R}_2,\omega) & \cdots & \mathbf{S}(\mathbf{R}_2,\mathbf{R}_n,\omega) \\ \vdots & & & \\ & \vdots & \vdots & \vdots \\ \mathbf{S}(\mathbf{R}_n,\mathbf{R}_1,\omega) & \mathbf{S}(\mathbf{R}_n,\mathbf{R}_2,\omega) & \cdots & \mathbf{S}(\mathbf{R}_n,\mathbf{R}_n,\omega) \end{bmatrix} . \tag{3}$$

In this matrix, $\alpha(\omega)$ represents the effective dipolar polarizability of an atom belonging to the tip apex and the dyadic tensor $\mathbf{S}$ is the field susceptibility associated with the coated surface [cf. Sec. II B]. The positions of these atoms are defined by

$$\mathbf{R}_j=\mathbf{R}_0+\mathbf{L}_i , \tag{4}$$

where the vectors $\mathbf{L}_i$ represent the atom locations with respect to the position $\mathbf{R}_0$. The dispersion relation (2) is sufficient for determining the tip-sample dispersion potential energy

$$U_d(\mathbf{R}_0)=\frac{\hbar}{2\pi}\int_0^\infty \ln\{\det[\underline{I}-\underline{B}(\mathbf{R}_0,iu)]\}du . \tag{5}$$

For interatomic distances beyond the repulsive regime each matrix element of $\underline{B}(\mathbf{R}_0,iu)$ remains small with respect to the unit. It is then possible to perform the following expansion:

$$U_d(\mathbf{R}_0)=-\frac{\hbar}{2\pi}\int_0^\infty \sum_{m=1}^{\infty}\frac{1}{m}\mathrm{Tr}[\underline{B}^{(m)}(\mathbf{R}_0,iu)]du \tag{6}$$

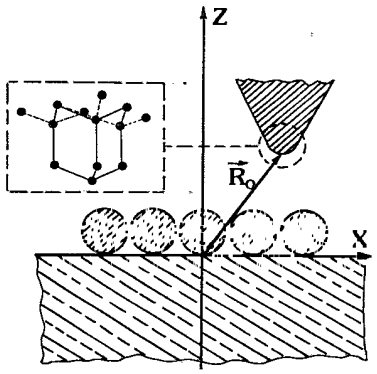

FIG. 1. Geometry of an AFM tip placed in interaction with a covered substrate. The dashed circles schematize adsorbed polyatomic molecules like fullerenes. The vector $\mathbf{R}_0=(X_0,Y_0,Z_0)$ defines the position of the apex atom of the probe tip. The atomic structure of the diamond tip apex used in the model is built on the basis of a (111) orientation which means that the second layer of atoms is very close (0.5 Å) to the apex atom.

in which $\underline{B}^{(m)}$ represents the matrix product of the mth order. It may be seen that the first term ($m=1$) corresponds to the direct coupling between each element inside the tip and the coated sample. We now need to specify the form of the dyadic tensor $\mathbf{S}$ used to characterize the dynamical response of the coated surface.

B. Field susceptibility of a coated surface

The growing interest in the study of natural or artificial structures stabilized by a corrugated surface calls for specific models adapted to the low symmetry of such systems. In this part the field susceptibility of a reference system (the surface) covered by a finite number of polyatomic molecules is derived from a sequence of Dyson's equations. For a large number of interacting particles, i.e., all atoms composing the adsorbed molecules, we find it more adequate to derive the field susceptibility by using a fully self-consistent iterative scheme. In order to illustrate this procedure we consider a system composed of (N) atoms interacting with a surface. Note that for a set of n_1 identical molecules formed of n_2 atoms, the total number N of atoms is $n_1 n_2$. The field susceptibility associated with the first atom is found by application of Dyson's equation[20]

$$\mathbf{S}_1(\mathbf{r},\mathbf{r}',\omega)=\mathbf{s}_0(\mathbf{r},\mathbf{r}',\omega)+\alpha_a(\omega)\cdot\mathbf{s}_0(\mathbf{r},\mathbf{r}_1,\omega)\cdot\mathcal{A}_1(\omega)\times\mathbf{s}_0(\mathbf{r}_1,\mathbf{r}',\omega)\ . \tag{7}$$

In this equation, the index (1) refers to the first atom of the first adsorbate and $\alpha_a(\omega)$ represents its dynamical polarizability. The dyadic tensor $\mathbf{s}_0$ represents the field susceptibility associated with the substrate alone. This quantity describes how a punctual dipolar source field is modified at the proximity of the surface. Various analytical forms of this response function are available in the literature.[19] Finally, the (3×3) tensor $\mathcal{A}_1$ is the result of a small matrix inversion

$$\mathcal{A}_1(\omega)=[\mathbf{I}-\alpha_a(\omega)\cdot\mathbf{s}_0(\mathbf{r}_1,\mathbf{r}_1,\omega)]^{-1}\ . \tag{8}$$

In a similar way, the field susceptibility labeled $\mathbf{S}_2$ associated with the two first atoms of the molecular aggregate can be deduced from the knowledge of $\mathbf{S}_1$. This leads to

$$\mathbf{S}_2(\mathbf{r},\mathbf{r}',\omega)=\mathbf{S}_1(\mathbf{r},\mathbf{r}',\omega)+\alpha_a(\omega)\cdot\mathbf{S}_1(\mathbf{r},\mathbf{r}_2,\omega)\cdot\mathcal{A}_2(\omega)\times\mathbf{S}_1(\mathbf{r}_2,\mathbf{r}',\omega)\ . \tag{9}$$

At this stage the matrix $\mathcal{A}_2$ is built by replacing $\mathbf{s}_0$ by $\mathbf{S}_1$ in Eq. (8). By repeating this procedure, it is thus possible to derive the field susceptibility $\mathbf{S}_N$ of a discrete system formed of N atoms from the field susceptibility $\mathbf{S}_{N-1}$ of a system composed of ($N-1$) atoms. This leads to

$$\mathbf{S}_N(\mathbf{r},\mathbf{r}',\omega)=\mathbf{S}_{N-1}(\mathbf{r},\mathbf{r}',\omega)+\alpha_a(\omega)\cdot\mathbf{S}_{N-1}(\mathbf{r},\mathbf{r}_N,\omega)\cdot\mathcal{A}_N(\omega)\times\mathbf{S}_{N-1}(\mathbf{r}_N,\mathbf{r}',\omega)\ . \tag{10}$$

Such an algorithm avoids the numerical inversion of a very large matrix ($3N\times3N$). It reduces the self-consistent problem to a succession of small matrix (3×3) inversions. This iterative scheme is therefore relevant for all studies concerned with a great number of degrees of freedom because it is much less critical in terms of time consumption. It is particularly well-suited for considering low-symmetry systems for which analytical expressions rapidly become intractable. Moreover, the use of this sequence of equations is not limited by numerical accuracy because the field susceptibility avoids the problem of self-energy. From Eq. (10) it is possible to fill the dynamical matrix $\underline{B}$ [cf. Eq. (3)] by using the different components taken by $\mathbf{S}_N$ for all possible couples of position $\{\mathbf{R}_i,\mathbf{R}_j\}$ occupied by the atoms composing the AFM tip.

III. APPLICATION TO A SPECIFIC SYSTEM: C_{60} MOLECULES ON A GOLD SURFACE

Since the discovery of fullerene molecules[21] and of an efficient method[22] for its bulk synthesis, the field of research on these carbon particles has recently grown dramatically. Among the different experimental techniques used to characterize fullerene materials, local probe methods including AFM and STM appear to be useful complementary techniques. Thus C_{60} thin films of ordered monolayers have been imaged with the STM on many substrates.[23] Moreover, isolated fullerene molecules on Au(110) (Ref. 24) and polycrystalline Pt (Ref. 25) have been studied with an STM and the interpretation of the images has been recently proposed by Chavy, Joachim, and Altibelli.[26] Atomic force microscopy also appears to be an interesting alternative for investigating such systems. In contrast to STM, AFM can directly measure tip-sample forces and thereby produces information on the spatial distribution of the adsorbed fullerene molecules. As described in Ref. 7, the C_{60} molecules on Au(110) often appear grouped in a hexagonal arrangement displaying no atomic-scale features on the top of the molecules. Very recently, AFM of C_{60}/C_{70} single-crystal fullerenes has been reported. The adsorbed molecules are arranged either in hexagonal or cubic packing[8] and the measurement must be performed using very low contact forces (lower than 0.4 nN) to prevent destruction or deformation of the soft monolayer. The understanding of the physical mechanisms occurring during the imaging process calls for extensive numerical simulations of such systems. The origin of contrast in AFM appears to be a complex mixture of sample deformation, tip apex composition and structural properties of the probe-sample system. In this section, we present numerical calculations involving tip-sample force [relations (1) and (5)] deduced from the sequence of Dyson's equations described in Sec. II B. The system studied here consists of a set of (p) C_{60} molecules deposited on a perfectly plane gold surface. In a first step, the atoms composing the molecules and the molecules themselves will be frozen in their equilibrium positions. This approximation is relevant with respect to all experiments where the surface is covered by a complete fullerene monolayer and in which the imaging process is performed with a very low contact force. So for such weak scanning forces, one can expect the molecules to keep their equilibrium sites for each tip-sample

configuration. First, we define the different response functions used to describe the substrate and the adsorbed molecules.

(i) *The substrate.* The various expressions for the dispersive energy given in previous sections have been obtained without restrictive assumptions about the description of the substrate. The specificity of the surface enters the Eqs. (5) and (6) through the field susceptibility $\mathbf{s}_0$. From results available in the literature, the real profile of the surface could be included in our application without formal difficulties. However, for the sake of clarity, we will restrict our study to the case of a perfectly planar surface. In such a model the field susceptibility $\mathbf{s}_0(\mathbf{r},\mathbf{r}',iu)$ can be expressed in terms of the local dielectric constant $\epsilon(iu)$ of the material at imaginary frequency. One has then[19]

$$\mathbf{s}_0(\mathbf{r},\mathbf{r}',iu)=\mathbf{T}(\mathbf{r},\mathbf{r}')+\mathbf{s}_s(\mathbf{r},\mathbf{r}',iu), \quad \text{if } (\mathbf{r}\neq\mathbf{r}') \tag{11}$$

and

$$\mathbf{s}_0(\mathbf{r},\mathbf{r}',iu)=\mathbf{s}_s(\mathbf{r},\mathbf{r},iu), \quad \text{if } (\mathbf{r}=\mathbf{r}') \tag{12}$$

where $\mathbf{T}(\mathbf{r},\mathbf{r}')$ labels the dipolar propagator in vacuum and $\mathbf{s}_s$ accounts for the presence of a surface.[19] Note that these two equations express the fact that it is not possible to couple a given atom with itself. Moreover in the absence of non-local effects in the substrate, the field susceptibility associated with the surface has a simple form because frequency and spatial dependence can be separated

$$\mathbf{s}_s(\mathbf{r},\mathbf{r}',iu)=\Delta(iu)\mathbf{F}(\mathbf{r},\mathbf{r}'), \tag{13}$$

where $\mathbf{F}$ is a dyadic tensor describing the spatial variation of $\mathbf{s}_s$,

$$\mathbf{F}(\mathbf{r},\mathbf{r}')=\frac{1}{2\pi}\int_{-\infty}^{\infty}\int_{-\infty}^{\infty}\frac{d\mathbf{k}}{k}\mathbf{K}\mathbf{K}^* \times\exp[-i\mathbf{k}\cdot(l-l')] \times\exp[-k(z+z')] \tag{14}$$

with $\mathbf{K}=(i\mathbf{k},-k)$, $\mathbf{r}=(l,z)$, and $\mathbf{r}'=(l',z')$. In Eq. (13), Δ represents the nonretarded reflection coefficient of the surface at imaginary frequency

$$\Delta(iu)=\frac{[\epsilon(iu)-1]}{[\epsilon(iu)+1]}. \tag{15}$$

Note that useful model formulas exist[27] where one may assume a Lorentzian form to describe this reflection coefficient.

(ii) *The adsorbate.* For ideal C_{60} molecules the spatial arrangement of carbon atoms can be found in Ref. 28. Moreover in the context of van der Waals dispersive interactions, analytical forms for the dynamical polarizabilities $\alpha(iu)$ and $\alpha_a(iu)$ at imaginary frequency are needed. For C_{60} carbon atoms we have used recent data given by Vidali *et al.*[29] for the (1000) face of graphite. Note that these data, when applied to van der Waals interactions between two isolated C_{60} molecules, give numerical results in striking agreement with the continuum model recently developed by Lambin, Lucas, and Vigneron.[30]

IV. NUMERICAL RESULTS

The system considered here consists of an aggregate of seven C_{60} molecules placed at the nodes of a hexagonal lattice in the vicinity of a gold surface. As far as we know, no experimental data are available for the equilibrium distance D_{eq} of a single C_{60} ball on such metallic surfaces. Recently, this distance was estimated by using the MM2 molecular mechanical routine.[26] For the (110) face of gold this procedure leads to $D_{eq}=6.5$ Å. The distance D in a plane parallel to the substrate between two adjacent molecules is found to be equal to 9.95 Å. This value has been determined by introducing the short-range part described in Eq. (1). Let us note that the determination of this equilibrium distance has been performed by accounting for many-body effects at any order in the dispersion energy calculation of two C_{60} adsorbed molecules. This value is very close to the fullerite nearest-neighbor distance (10.04 Å).[30]

In Fig. 2, the variation of both tip-sample energy $U=U_r+U_d$ and the corresponding normal force is drawn as a function of the approach distance Z_0. Three typical sites labeled (a), (b), and (c) have been investigated. It may be seen that the equilibrium position of the tip apex (calculated for $F=0$), varies from 12.75 to 10.2 Å as the tip is moved from the top site to the hollow one. Moreover, above the hollow site (c) the binding energy is maximum and reaches about 1 eV which is consistent with the number of nearest neighbors seen by the tip extremity in such a spatial configuration. In a similar way, the positions of the maxima of the normal force in the attractive range, vary between 10.7 and 13.15 Å. This means that the attractive zone is shifted 2.08 Å away from the hollow site to the top site. Finally, let us recall that this analysis assumes that all mechanical deformations of the molecular pattern due to the interaction with the probe are weak.

From the knowledge of the function $U(X_0,Y_0,Z_0)$, it is possible to study the evolution of the tip-sample energy as the probe tip is scanning the sample. Figure 3 presents two series of equipotential curves $U(\mathbf{R}_0)=\text{const}$. These curves have been obtained by calculating the variation of the energy U in a plane ($Z_0=$const.) parallel to the surface. The scanned area is (40×40) Å and the geometrical parameters are the same as in Fig. 2. Two different approach distances have been investigated and in each case the energy varies by steps of 10 meV. As illustrated by the two van der Waals energy patterns (3a) and (3b), the density of iso-energy lines varies dramatically when the tip-sample distance decreases. So, above the molecule located at the very center of the pattern, the energy contrast increases by a factor 2.8 for a variation of 1 Å. This high sensitivity with respect to the approach distance will be useful for imaging fullerene molecules by working in the attractive range.

We now address the question of the tip-sample force and imaging process. Figure 4 presents two sequences of constant-distance AFM images calculated in the attractive range by scanning an area of (20×20) Å^2 centered around the origin. For each spatial configuration (X_0,Y_0) the function U is calculated for a small number

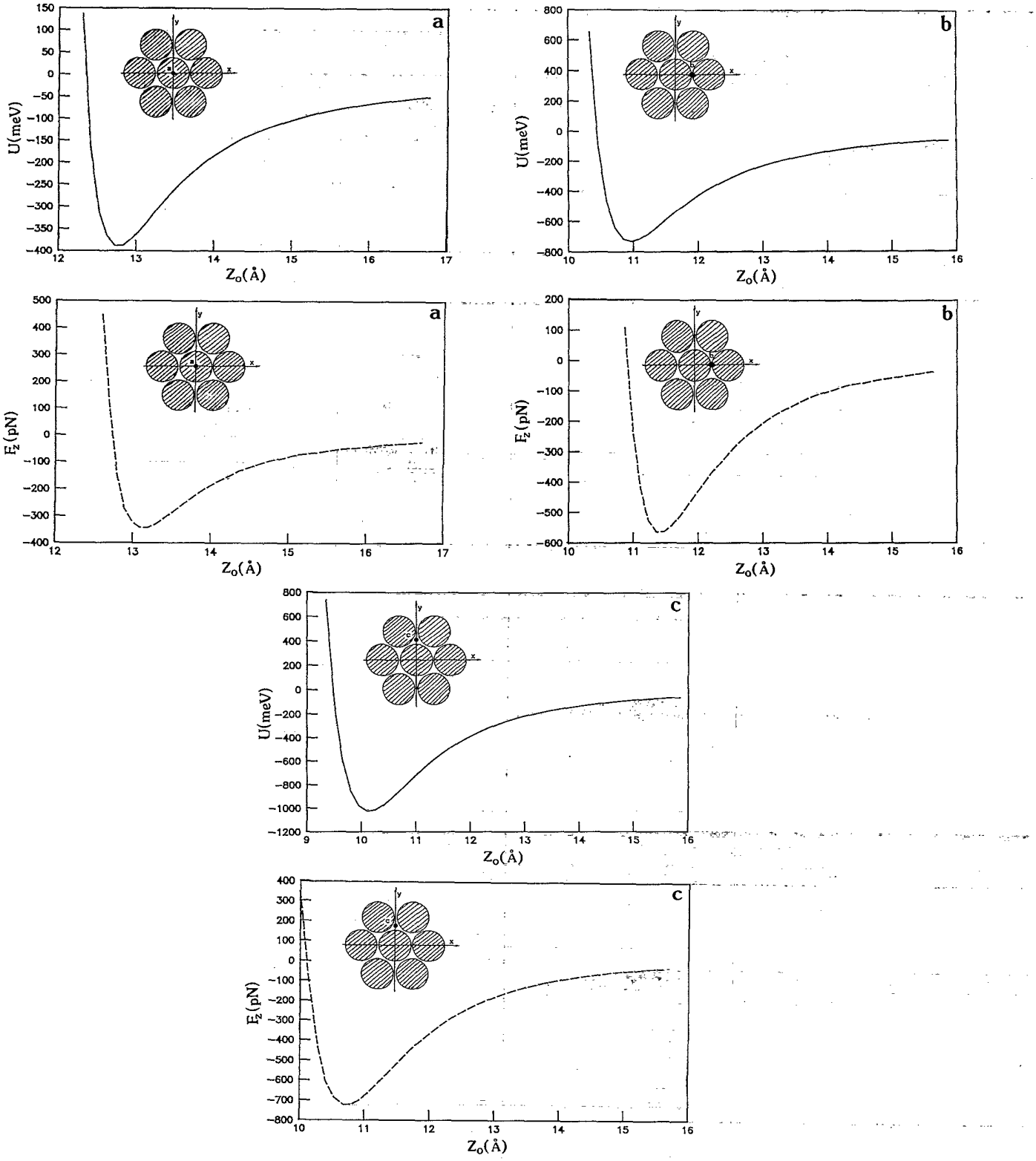

FIG. 2. Illustration of the variation of both tip-sample energy (solid curves) and tip-sample force (dashed curves) as a function of the approach distance Z_0 calculated above three different sites. The object is a set of seven C_{60} molecules deposited on a gold surface and organized on the substrate as an hexagonal pattern. The approach distance D between two neighboring molecules is 9.95 Å. This value has been determined by introducing the short-range part described in Eq. (1) (with $C_{12}=1.825\times10^6$ a.u.). Note that the determination of this equilibrium value has been performed by accounting for many-body effects at any order in the dispersion energy calculation. The gold substrate is assumed to be a continuous medium and the adsorption distance between fullerenes and surface is chosen equal to 6.5 Å. Three typical sites have been considered: (a) $X_0=0$ and Y_0 (top site). (b) $X_0=D/2$ and $Y_0=0$. (c) $X_0=0$ and $Y_0=D/3^{1/2}$ (hollow site).

of points located around Z_0. The function $U(Z)$ is then fitted from these points by a polynomial in Z. The Z-force component is calculated at the point Z_0 from this polynomial. We have used five values of Z to fit $U(Z)$. As illustrated in Fig. 4, the two-dimensional maps calculated in the attractive range display no intramolecular contrast on the top of the molecule, but then in each case all molecules of the pattern appear well localized in the image. Moreover, as expected, the amplitude of the corrugation forces decreases when the tip draws away from the sample. This decrease reaches about 80*pN* when the tip moves from 14 to 14.5 Å. In any case, these topographies clearly indicate that the amplitude variation of the lateral attractive dispersion force in this range is sufficiently large to image individual fullerene molecules by recording force magnitudes accessible with recent experimental devices.[7,8] To complete our study, we present in Fig. 5 a series of isoforce curves computed in a plane $Z_0=15.5$ Å. The force in the image varies from 22 to 78 pN by steps of 2 pN. For this approach distance, the average force reaches about 40 pN above the saddle points of the pattern and the predicted corrugation force $\Delta F \simeq 56$ pN is of the same order of magnitude as the AFM measurements performed by Sarid *et al.*[7] on the same system.

In the AFM constant force mode of imaging, the tip is scanned across the surface with a constant loading force applied to the apex. Since the tip is attached to or grown from a cantilever, this force induces an elastic deformation of the cantilever during the scan. Thus, when the tip is displaced along the sample under test, it follows the contour of the object and the images are obtained by measuring the deflection of the cantilever. A simulation of this operating mode is given in Fig. 6 where we have calculated the trajectory of the tip apex for two different loading forces (80 and 100 pN). These forces were chosen

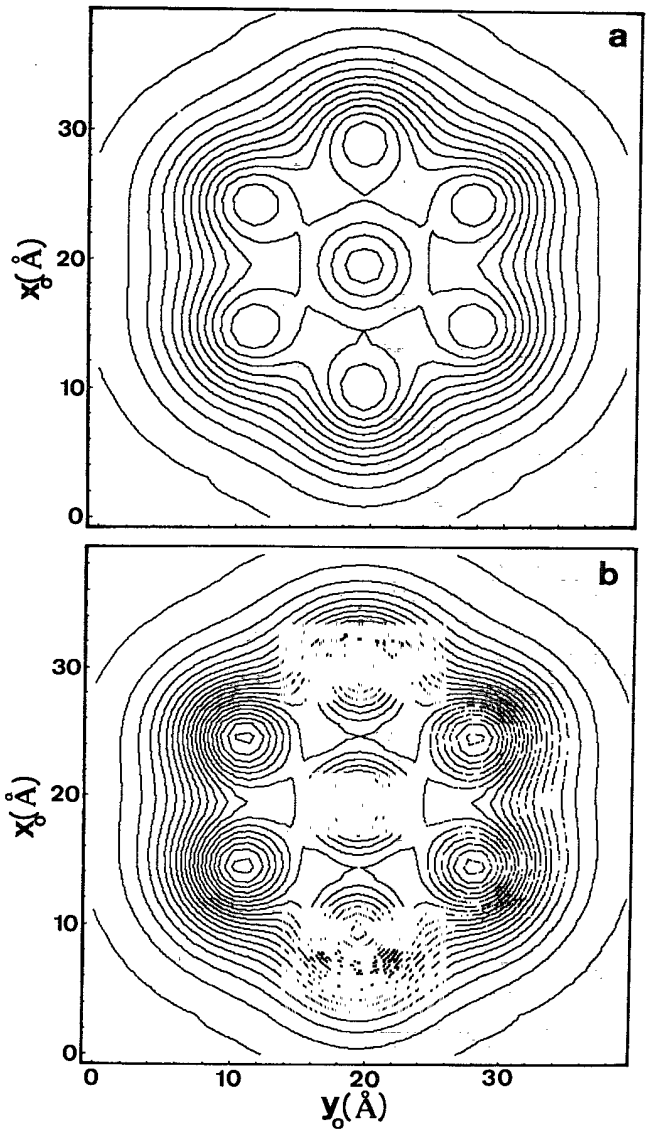

FIG. 3. Representation of two sequences of isoenergy curves $U(\mathbf{R}_0)$=const experienced by the probe tip above a set of seven C_{60} molecules physisorbed on a gold surface. The geometrical parameters are the same as in Fig. 2. The calculation is performed in a plane parallel to the surface (Z_0=const) and the scanned area is (40×40) Å^2. (a) $Z_0=14.5$ Å; (b) $Z_0=13.5$ Å.

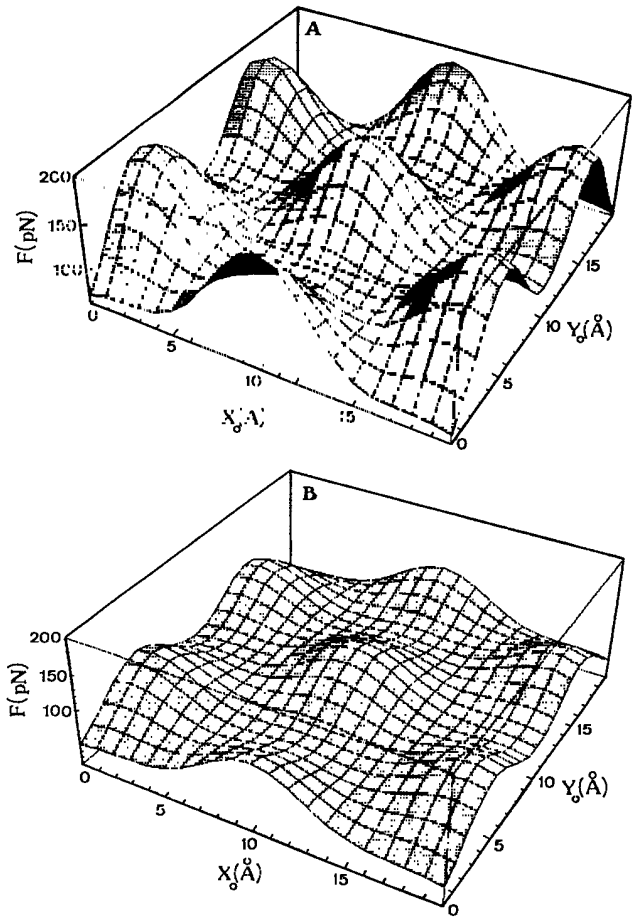

FIG. 4. Two sequences of constant-distance AFM images calculated in the attractive range. The sample is the same as the one described in Figs. 2 and 3. The forces are given in pN (10^{-12} N) and the scanned area is (20×20) Å^2. (a) $Z_0=14$ Å; (b) $Z_0=14.5$ Å.

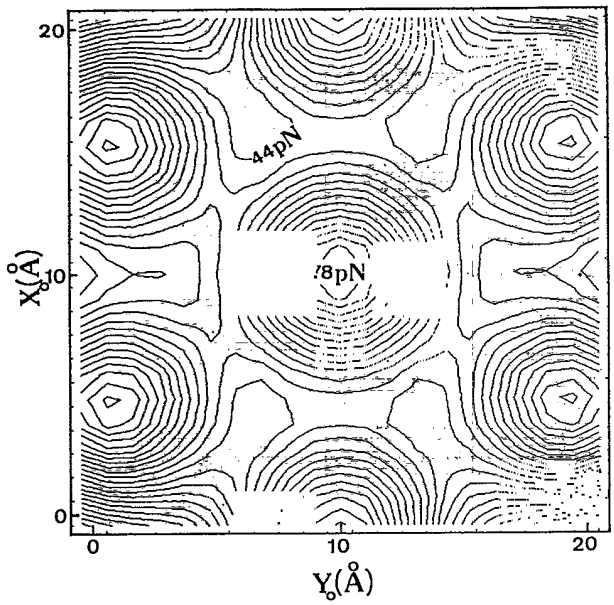

FIG. 5. Representation of an ensemble of isoforce curves calculated in the plane $Z_0 = 15.5$ Å located in the attractive range. As in previous calculations the sample consists of a set of seven C_{60} molecules and the scanned area is (20×20) Å^2. The force varies from 22 to 78 pN in steps of 2 pN.

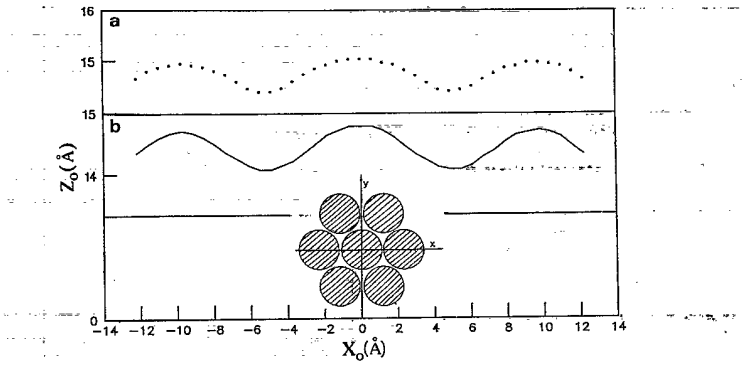

FIG. 6. Constant-force AFM scans calculated along the $0X$ axis: (a) The loading force $F_{ap} = 80$ pN; (b) $F_{ap} = 100$ pN.

in such a way that the tip apex does not deform the C_{60} molecule. This can be verified in Fig. 2(a) where for $F_z \leq 100$ pN, the tip apex altitude is larger than 15 Å. In this case, there is more than a 5-Å distance separation between the last top C_{60} carbon atom and the tip apex end atom. This is a distance large compared to the van der Waals radius of two carbon atoms. It is clear from our calculation that the deflection amplitude occurring above the spheres is very sensitive to the magnitude of the applied force F_{ap}. For example for $F_{ap} = 100$ pN, the corrugation reaches 0.65 Å which is found to be in good agreement with experimental measurements.[8]

V. SUMMARY

In this work we have investigated different manifestations of the interaction between a realistic probe-tip and a small array of adsorbed fullerene molecules. The long range part of the tip-sample interaction has been described in the framework of the coupled mode method expressed in terms of the field susceptibility of the covered surface. Assuming the response of the naked substrate is known via a given field susceptibility, we have proposed a numerical algorithm leading to a general description of the surface when it is converged with a great number of particles. Such a procedure avoids the usual extensive computer time and memory allocation required by matrices of large size. As illustrated by the applications detailed in Sec. IV, the present approach appears to be an efficient tool for modeling tip-sample coupling that occurs in atomic force microscopy. Numerical applications on C_{60} adsorbed molecules give results in good agreement with recent experimental data.

ACKNOWLEDGMENTS

The authors express their sincere thanks to A. A. Lucas and to Ph. Lambin for numerous interesting discussions. One of us (A.D.) gratefully acknowledges the Walloon Ministry for Research and Technology (Brussels) for financial support. Laboratoire de Physique Moléculaire is Unité de Recherche Associée No. 772 and CEMES is Unité Propres de Recherche No. 8011 au CNRS.

[1]H. Rohrer, Ultramicrosc. **42-44**, 1 (1992).
[2]G. Binnig, Ultramicrosc. **42-44**, 7 (1992).
[3]G. Binnig, C. F. Quate, and Ch. Gerber, Phys. Rev. Lett. **56**, 930 (1986); O. Marti, H. O. Ribi, B. Drake, T. R. Albrecht, C. F. Quate, and P. L. Hansma, Science **239**, 50 (1988).
[4]E. Meyer, Progr. Surf. Sci. **41**, 1 (1992).
[5]D. Sarid, *Scanning Force Microscopy* (Oxford University Press, New York, Oxford, 1991).
[6]D. Rugar and P. Hansma, Phys. Today **43**(10), 23 (1990).
[7]D. Sarid, T. Chen, S. Howells, M. Gallagher, L. Yi, D. L. Lichtenberger, K. W. Nebesney, C. D. Ray, D. R. Huffman, and L. D. Lamb, Ultramicrosc. **42-44**, 610 (1992).
[8]P. Dietz, P. K. Hansma, K. Fostiropoulos, and W. Krätschmer, Appl. Phys. Lett. **60**, 62 (1992); Appl. Phys. A **56**, 207 (1993).
[9]F. F. Abraham and I. P. Batra, Surf. Sci. **209**, L125 (1989); S. Ciraci, A. Baratoff, and I. P. Batra, Phys. Rev. B **41**, 2763 (1990); S. Ciraci, E. Tekman, M. Gökçsdag, I. P. Batra, and A. Baratoff, Ultramicrosc. **42-44**, 163 (1992).
[10]W. Zong, G. Overney, and D. Tomanek, Europhys. Lett. **15**, 49 (1991); G. Overney, D. Tomanek, W. Zang, Z. Sun, H. Miyazaki, S. D. Mahanti, and H. J. Gütherrodt, J. Phys. C **4**, 4233 (1992).
[11]C. Girard, Phys. Rev. B **43**, 8822 (1991); C. Girard, S. Maghezzi, and D. Van Labeke, Surf. Sci. **234**, 181 (1990).
[12]U. Hartmann, Phys. Rev. B **42**, 1541 (1990); **43**, 2404 (1991).

[13]E. M. Lifshitz, Zh. Eksp. Teor. Fiz. **29**, 94 (1956) [Sov. Phys. JETP **2**, 73 (1956).
[14]C. Girard, A. Dereux and O. J. F. Martin (unpublished).
[15]H. Tang, C. Joachim, and J. Devillers, Surf. Sci. **291**, 439 (1993).
[16]A. Lakhlifi and C. Girardet, J. Mol. Struct. **110**, 73 (1984).
[17]B. Linder and D. A. Rabenold, Adv. Quantum Chem. **6**, 203 (1972).
[18]N. G. Van Kampen, B. R. A. Nijboer, and K. Schram, Phys. Lett. **26A**, 307 (1968).
[19]C. Girard and X. Bouju, J. Chem. Phys. **95**, 2056 (1991).
[20]E. N. Economou, *Green's Functions in Quantum Physics,* 2nd ed. (Springer, Berlin, 1983).
[21]H. W. Kroto, J. R. Heath, S. C. O'Brien, R. F. Curl, and R. E. Smalley, Nature (London) **318**, 162 (1985).
[22]W. Krätschmer, L. D. Lamb, K. Fostiropoulos, and D. R. Huffman, Nature (London) **347**, 354 (1990).
[23]Y. Z. Li, M. Chander, J. C. Patrin, J. H. Weaver, L. P. F. Chibante, and R. E. Smalley, Science **253**, 429 (1991).
[24]Y. Zhang, X. Gao, and M. J. Weaver, J. Phys. Chem. **96**, 510 (1992).
[25]H. P. Lang, V. Thommen-Geiser, J. Frommer, A. Zahab, P. Bernier, and H. J. Güntherrodt, Europhys. Lett. **18**, 29 (1992).
[26]C. Chavy, C. Joachim, and A. Altibelli, Chem. Phys. Lett. (to be published).
[27]G. Vidali and M. W. Cole, Surf. Sci. **110**, 10 (1981).
[28]W. F. David, R. M. Ibberson, J. C. Matthewman, K. Prassides, T. J. S. Dennis, J. P. Hare, H. W. Kroto, R. Taylor, and D. R. M. Walton, Nature **353**, 167 (1991).
[29]G. Vidali, G. Ihm, H. Y. Kim, and M. W. Cole, Surf. Sci. Rep. **12**, 135 (1991), and references therein.
[30]Ph Lambin, A. A. Lucas, and J-P. Vigneron, Phys. Rev. B **46**, 1794 (1992).